CERN-LCGAPP-2012-01
April 25, 2012
Version 1.0

Simplified Calorimeter: shower moments

Andrea Dotti (andrea.dotti@cern.ch)

Contents

1 Introduction

In this note we describe the use of *shower moments* to present in a compact way properties of showers induced by high energy primaries in calorimeters.

This work has been developed in the context of the *SimplifiedCalorimeter* testing suite developed for the GEANT4 simulation toolkit. The testing suite implements different types of calorimeter technologies in a simplified setup (no read-out, large dimensions). The materials and segmentations used are similar to the calorimeters of LHC as well as to some calorimeters from past experiments (HERA) as well as future calorimeters currently in the R&D

phase (CALICE). The testing suite is used to validate and compare the different models available in GEANT4 (with data when available), it is also used as a regression testing suite to validate new developments.

The typical calorimetric observables (response, resolution, shower shapes) are measured and analyzed.

In this note we concentrate our attention on a new approach to measure the shower dimensions: we describe the implementation of the shower moments, with details on the presented algorithm. Results will be present with the goal to show the sensitivity of the method. We will not go in the details of the comparison of different physics lists and different versions of GEANT4 .

The appendix contains details of the developed code. It is intended to serve as a guide to extend the application to include new shower moments.

2 Definition of Shower Moments

The detailed study of hadron interaction with calorimeters can be studied in terms of shower shapes. Usually the longitudinal and lateral profile are calculated as fraction of energy in different sections of the calorimeter (*shower profile*).

Detailed analysis of the shower profiles has been carried out for different physics lists in the past years and results have been presented in [1] and [2]. The general conclusions is that the effect of intra nuclear cascade models, in particular with the Bertini model, is to make showers wider, in the right direction with respect to test-beam data. The Fritiof model used in `FTF_BIC` and `FTFP_BERT` is a promising alternative to `QGSP_BERT` , in particular for the longitudinal profile of protons.

The definition of shower moments has been inspired by the ATLAS *Local Hadron Calibration* method [3]. This method aims to calibrate, at the hadronic scale, the clusters (groups of calorimeter cells) recognizing the fraction of electromagnetic energy (energy deposits π^0) in a hadron induced shower. After reconstructing the cluster (trying to minimize the influence of the electronic noise), it is classified as electromagnetic or hadronic. Several *weights* are applied depending on the magnitude of different classifiers (for example: energy density in the cells, shower depth in the calorimeter) to correct for non-compensation, cracks and leakages.

In the context of this work we are not interested in the calibration of

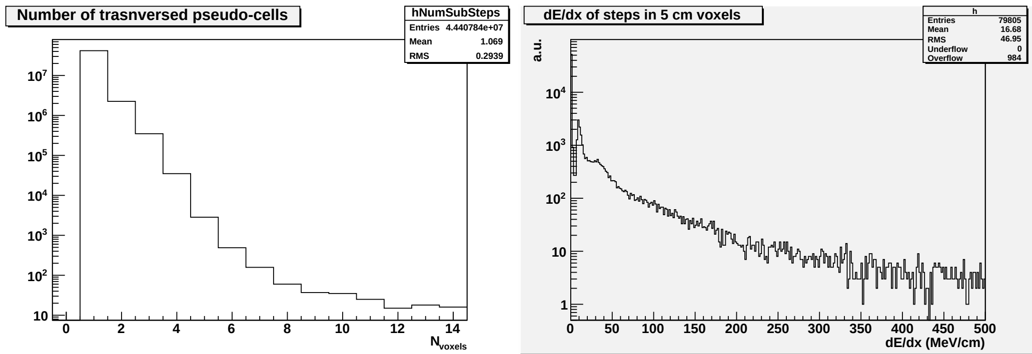

Figure 1: Left: distribution of the number of voxels spanned by a *G4Step*. Right: dE/dx deposits in the voxels.

the clusters, but we want to re-use some methodology to summarize, in few numbers, the characteristics and shape of the showers. Since we are dealing with a simplified calorimeter we do not have to deal with experimental issues like the contribution of noise, cracks and leakage.

We will show that the conclusions we make using this approach is equivalent to the ones obtained with the classical approach of the shower profiles. The moments method, has few benefits:

- It leads to a simplified classification of each shower with its shape defined by a (relatively small) set of parameters
- The shower moments parameters, calculated for each shower, allow for a direct correlation with quantities of interest at the microscopic level (number and type of hadronic interactions in the shower, fraction of energy carried by the different particle species, see section 7)
- The moments are only weakly dependent on the segmentation used to calculate moments themselves

2.1 Algorithm

Since no electronic noise is simulated, we are able to define the *cluster* as the set of all cells with $E > 0$, the energy of the cluster is thus simply defined as:

$$E_{cluster} = \sum_{c \in \{cells\}} E_c \tag{1}$$

This, by definition, is the total energy deposited by the impinging hadron in the calorimeter. We are left with the need of defining the *cells*. Our setup is already equipped with a *ReadOut Geometry* used to calculate the shower profile. This is defined dividing the entire calorimeter in as a series of concentric tubes. This segmentation is particular useful, for its phi-symmetry, to calculate the shower profiles, but we prefer to add a second segmentation made of boxes (*voxels*) that define a three dimensional *mesh*: an envelope of the calorimeter. By default the voxels have a size of $5 \times 5 \times 5$ cm^3.

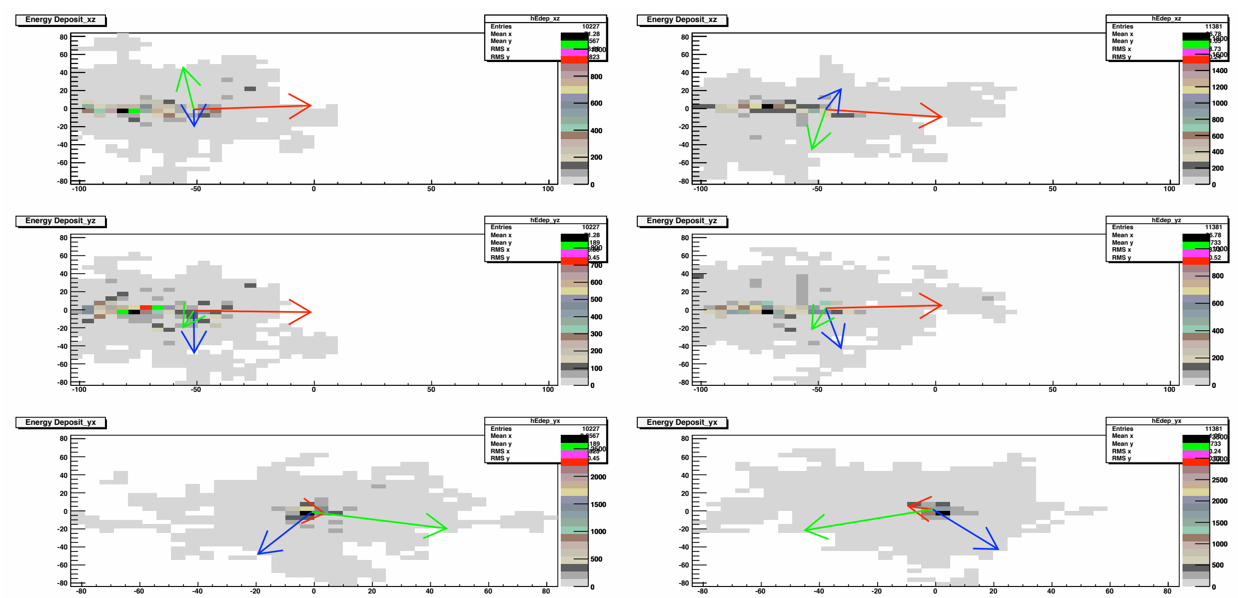

Figure 2: Examples of showers for two events . The top plots shows the projection in the xz plane, the middle plots for the yz projection and the bottom ones show the yx projection. Beam axis is along z axis. The colored arrows show the principal axes of the showers.

For each *G4Step* we search which voxels are spanned and we accumulate, for each event, the energy deposited. We note that it is possible that a single *G4Step* spans more than one voxel: the left plot of Figure 1 shows the distribution of the number of voxels crossed by each *G4Step*s. The energy deposit in each voxel is then calculated as:

$$\begin{aligned} \Delta E_v &= \frac{dE}{dx} \times \Delta L_v \ , \ v \in \{voxels\} \\ \frac{dE}{dx} &\approx \frac{\Delta E_{G4Step}}{\Delta L_{G4Step}} \end{aligned}$$

Where ΔL_v is the length of the $G4Step$ in the voxel v. The distribution of the dE/dx is shown in the right plot of 1.

Since the voxels are quite small the hadronic shower is sampled with high granularity, as shown in Figure 2. The figures show the projections in the different planes of two different showers originating from impinging protons at 20 GeV.

The shower moments are calculated starting from the energy deposits in the mesh. A shower moment of degree n in an observable o is given by:

$$< o^n > = \frac{1}{E_{cluster}} \times \sum_{v \in \{voxels\}} E_v \ o_v^n \tag{2}$$

With $E_{cluster}$ defined by equation 1.

For many of the moments we use the shower axis is needed as reference. The axis is calculated via a principal component analysis. Defining:

$$\begin{aligned} M_{ij} &= \frac{1}{w} \sum_{v \in \{voxels\}} E_v^2 (i_v - < i >)(j_v - < j >) \\ i,j &\in \{x, y, z\} \\ w &= \sum_{v \in \{voxels\}} E_v^2 \end{aligned}$$

The principal axis are the eigenvectors of the symmetric matrix:

$$M = \begin{pmatrix} M_{xx} & M_{xy} & M_{xz} \\ M_{xy} & M_{yy} & M_{yz} \\ M_{xz} & M_{yz} & M_{zz} \end{pmatrix}$$

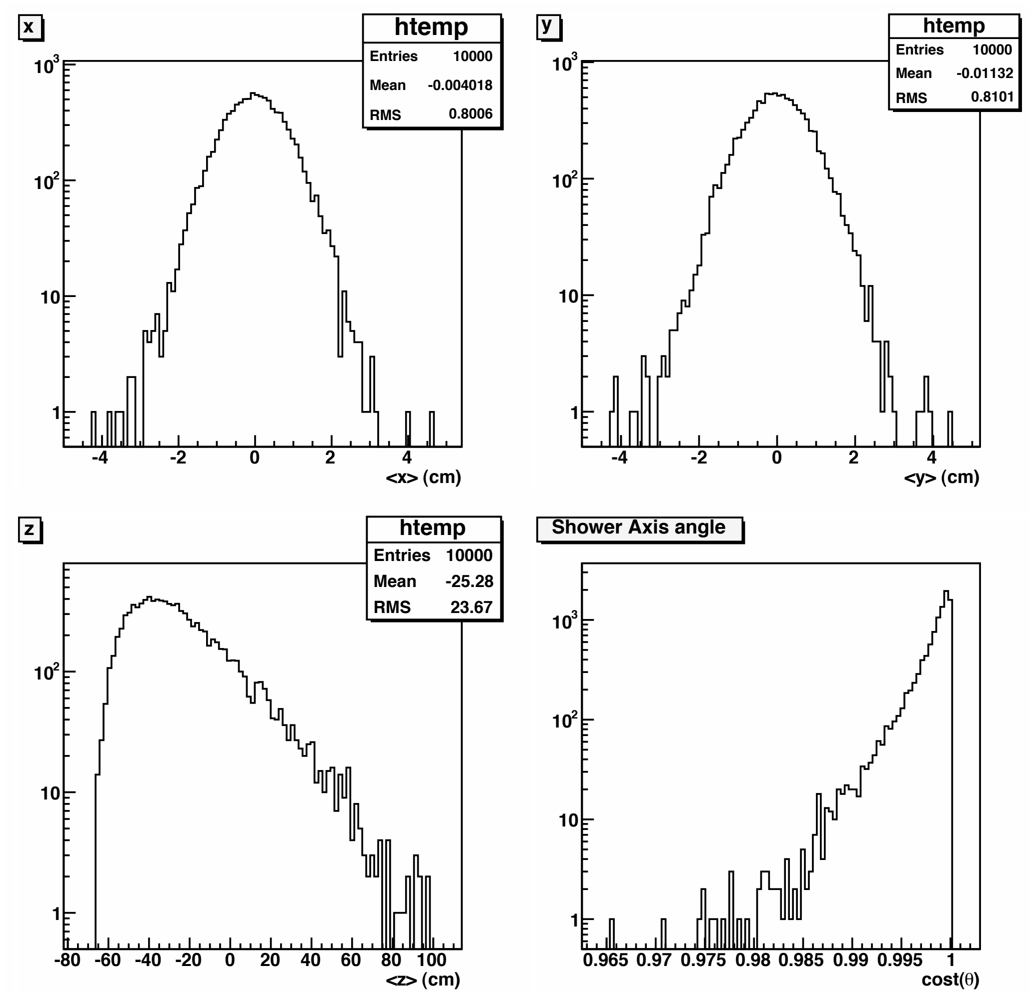

Figure 3: Distribution of the three components of the shower center $\vec{c}$ and of the angle between the shower axis $\vec{s}$ and the gun-to-center axis.

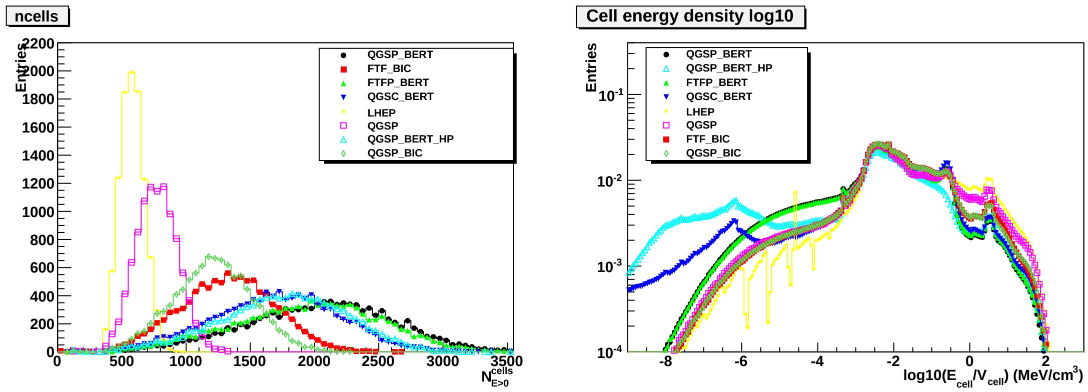

Figure 4: Number of voxels with $E > 0$ (right) and energy density ρ (left) for the different physics lists. Data obtained with a π^+ with $E_{kin} = 20$ GeV.

In Figure 2 the principal axis for the two showers are displayed with colored arrows. It should be noted that the axis are relative to the shower center

$$\vec{c} = (< x >, < y >, < z >) \tag{3}$$

The shower axis $\vec{s}$ which is closest to the direction pointing from the particle gun origin to the shower center (*gun-to-center*) is used as the shower axis. There can be (verified to be well below 1%) events in which the shower shape is such that the shower axis has a large angular deviation from the gun-to-center axis[1], in this case the gun-to-center axis is used as the shower axis.

Figure 3 shows the position of the shower center $\vec{c}$ and the cosine of the angle between the shower axis $\vec{s}$ and the gun-to-center axis. Since the primary particles have momentum along the z axis, the shower center is very close to the z axis: the $< x >$ and $< y >$ shower moments have an average value very close to 0 with a RMS of about 8 mm. The shower axis $\vec{s}$ is almost parallel to the gun-to-center axis (and thus to the z axis).

Once the vectors $\vec{c}$ and $\vec{s}$ have been defined for each voxel two quantities are calculated:

$$r_v = |(\vec{x}_v - \vec{c}) \times \vec{s}| \tag{4}$$
$$\lambda_v = (\vec{x}_v - \vec{c}) \cdot \vec{s} \tag{5}$$

[1]This can happen when the shower has a shape particularly spherical or that elongates in the x or y direction.

respectively: the distance of the voxel v from the shower axis and its distance from the shower center measured along the shower axis.

It is also useful to define the energy fraction in the *core* of the shower. To define this quantity two additional observable have been calculated for each shower using a *sliding window* algorithm approach[2]:

$$f^{max}_{n,m,l} = \frac{1}{E_{cluster}} \max_{w \in \{n \times m \times l\}} \left\{ \sum_{v \in \{w\}} E_v \right\} \quad (6)$$

$$f^{core}_{n,m} = \frac{1}{E_{cluster}} \max_{t \in \{n \times m\}} \left\{ \sum_{v \in \{t\}} E_v \right\} \quad (7)$$

for each shower the group of cells with size $n \times m \times l$ with maximum energy defines the core of the shower, similarly we search the group of cells in a tower of size $n \times m$.

For each event the following moments are calculated (in addition to the shower center and $E_{cluster}$):

- $< \rho >$: the first moment in the energy density[3] $\rho = E/V$, with V volume of the voxels.

- $< \rho^2 >$: the second moment in the energy density. Together with the previous moment these are sensitive to the electromagnetic fraction of the shower. Showers with larger fractions of energy carried by π^0 will have higher values of these shower moments.

- $< r >$ and $< r^2 >$: first and second moments on r (as defined in 4), these moments are sensitive to the shower lateral profile.

- $< \lambda^2 >$: second moment in λ (as defined in 5).

- λ_{center}: the distance of the shower center $\vec{c}$ from the calorimeter front face measured along the shower axis. This moment is sensitive to the depth of the shower, together with the previous moment allow for a description of the longitudinal profile of the shower.

[2]These quantities are also called moments. However they do not follow the general definition of moment. In a more general sense a moment is a parameter describing the shower, function of the energy deposited in each voxel.

[3]In the case of our simplified calorimeter from the definition of cluster moment and from the definition of the mesh follows that $< \rho >= V^{-1} < E^2 >$ and $< \rho^2 >= V^{-1} < E^3 >$ since the volume V of all voxels is a constant.

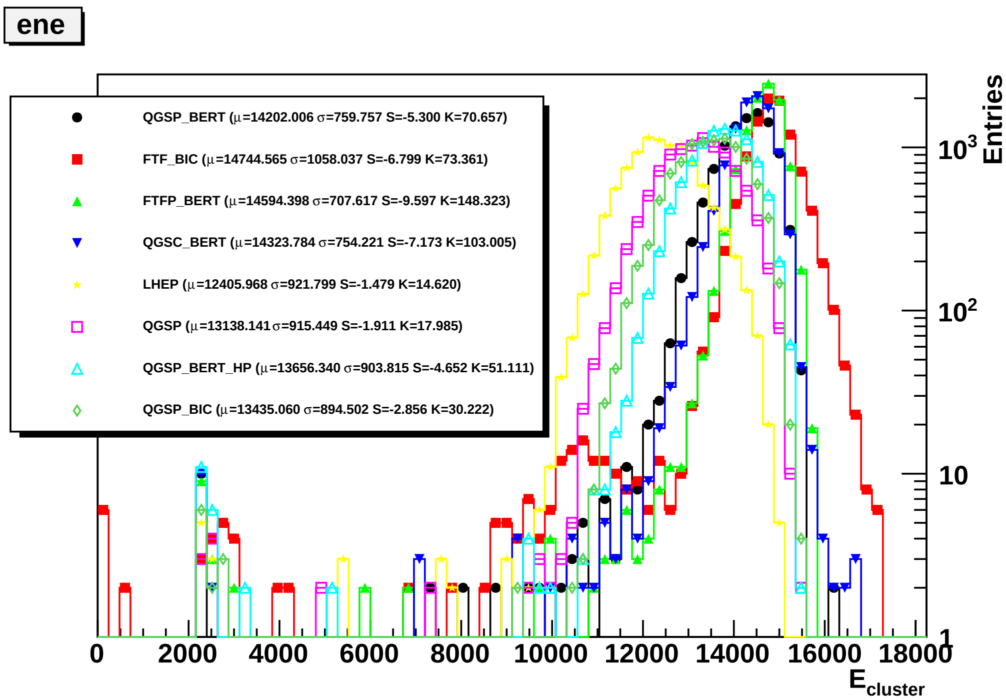

Figure 5: Total energy deposits for the different physics lists.

- $f^{max}_{2,2,2}$, $f^{max}_{3,3,3}$, $f^{max}_{5,5,5}$: the fraction of energy released in a group of cells of sizes $2 \times 2 \times 2$, $3 \times 3 \times 3$, $5 \times 5 \times 5$ (see Equation 6).
- $f^{core}_{2,2}$, $f^{core}_{3,3}$, $f^{core}_{5,5}$: the fraction of energy released in the sliding tower of sizes 2×2, 3×3, 5×5 (see Equation 7). Together with the previous set of moments these are sensitive to the dimension of the shower shape.

3 Results

The distributions for the number of voxels with $E > 0$ is shown in the left plot of Figure 4, this is a first, qualitatively, measurement of the size of the shower, large shower will have a higher number of voxels with energy deposits. `LHEP` and `QGSP` physics lists have the smallest shower, the inclusion of the Binary cascade models increase the size of the shower, the Bertini

$E_{cluster}$ (MeV)	Mean	Variance	Skewness	Excess Kurtosis
LHEP	12406	849798	-1.479	14.5657
QGSP	13138	838130	-1.9024	17.8895
QGSP_BIC	13435	800213	-2.8798	30.6165
QGSP_BERT	14202	577288	-5.2882	70.3345
QGSP_BERT_HP	13656	816962	-4.6336	50.7452
QGSC_BERT	14324	568906	-7.1694	103.2357
FTF_BIC	14745	1119555	-6.8207	73.6487
FTFP_BERT	14594	500771	-9.5910	148.2123

Table 1: Mean, variance, skewness and excess kurtosis of the total energy deposit obtained with 10000 events of π^+ with $E_{kin} = 20$ GeV.

intra-nuclear cascade models give the higher number of voxels interested by the shower (almost a factor 4 with respect the LHEP physics list).

The right plot of Figure 4 shows the distributions of the energy density for the different physics lists. The most probable value for the energy density is about 10 keV/cm^3, we can also note that the QGSP_BERT_HP and the QGSC_BERT physics lists have a tail to very low values of energy density. At the opposite we can find the LHEP and QGSP physics lists have more voxels with high energy density deposits.

3.1 Energy deposit moments

The distributions for the total energy deposit ($E_{cluster}$) for different physics lists are shown in Figure 5, the different physics lists are shown with different colors and markers, and Table 1 summarizes the results on the total energy deposits for the different physics lists.

The statistics[4] are calculated on ten thousands events of π^+ of $E_{kin} =$ 20 GeV. The `LHEP` (-5.57% with respect to `QGSP`) physics lists has the smallest energy deposit, followed by the `QGSP` physics list. The use of the Binary cascade increases the response (`QGSP_BIC` $+2.26\%$), Bertini (`QGSP_BERT_HP` $+3.94\%$, `QGSP_BERT` $+8.10\%$) increases even more the response in the calorimeter, `QGSC_BERT` ($+9.02\%$), `FTFP_BERT` (11.08%) and the `FTF_BIC` ($+12.23\%$) give the highest responses.

The variance of the different samples fluctuates around the `QGSP` physics list of about 40%, however no clear trend is visible.

From the analysis of the skewness and kurtosis we can understand the importance of the low energy tail. In this case the situation is similar to what we have observed for the mean value of the distributions. The `LHEP` and `QGSP` physics lists have the smaller tails, adding the intra nuclear cascade models increases the size of the tail (`QGSP_BIC`, `QGSP_BERT` and `QGSP_BERT_HP`), the most important tail is obtained with the `Fritiof` and `CHIPS` models.

The first and second moment on the energy density $< \rho >$ and $< \rho^2 >$ is another way to study the energy deposited. Figure 6 shows the distribution for the first (left) and second (right) energy density moments $< \rho >$ and $< \rho^2 >$. These distributions show a characteristic very long tail, present in all physics lists. The *core* of the distribution is at relatively low values of the energy density, while the tail can extend to very high values. The events in the tail represents showers in which the energy density fluctuates to considerably high values. This is characteristic of the electromagnetic component of the hadronic showers: the energy carried by π^0 is higher in this showers. We can show the correlation between energy deposit and density (left plot Figure 7), the events with higher $E_{cluster}$ populate the long tail of the energy density moment distribution. The right plot of Figure 7 shows the correlation between the electromagnetic component of the shower (energy deposited π^0) and $< \rho >$: the showers with higher value of $< \rho >$ have also

[4] Skewness is calculated as:

$$S = \frac{\sqrt{n(n-1)}}{n-2} \frac{\frac{1}{n}\sum_{i=1}^{n}(x_i - \overline{x})^3}{(\frac{1}{n}\sum_{i=1}^{n}(x_i - \overline{x})^2)^{3/2}}$$

The excess kurtosis is calculated as:

$$K = \frac{(n+1)n}{(n-1)(n-2)(n-3)} \frac{\sum_{i=1}^{n}(x_i - \overline{x})^4}{V^2} - 3\frac{(n-1)^2}{(n-2)(n-3)}$$

Where V is the unbiased estimator of the population variance.

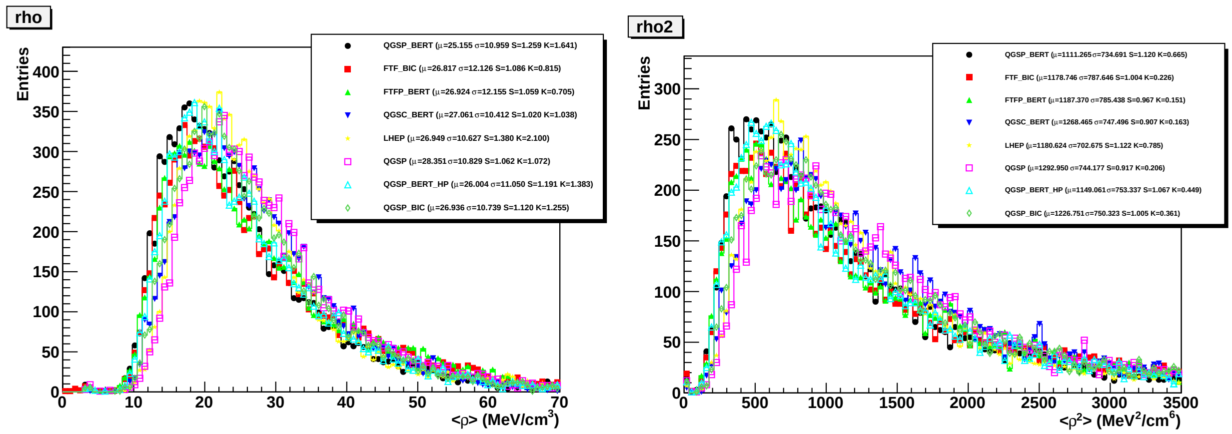

Figure 6: First (left) and second (right) energy density moments.

higher energy released by π^0.

Since it is difficult to appreciated the small differences between the different physics lists, it is more convenient to summarize the shape of the distributions through few numbers. Mean, variance, skewness and excess kurtosis have been calculated for each physics list.

For highly asymmetric distributions the characterization of the tail in terms of kurtosis and skewness is limited: we analyze this distributions in terms of quantiles.

The 50th (median), 84th and 98th percentile have been calculated for each distribution, we have then defined the following ratios:

$$R(50) = P_{50}/G_{50}(\mu, \sigma) \tag{8}$$

$$R(84) = P_{84}/G_{84}(\mu, \sigma) \tag{9}$$

$$R(98) = P_{98}/G_{98}(\mu, \sigma) \tag{10}$$

P_n is the nth percentile and $G_n(\mu, \sigma)$ is the nth percentile for a gaussian distribution with mean μ and standard deviation σ obtained from the original distribution. Being:

$$\phi(\frac{x-\mu}{\sqrt{2}\sigma}) = \frac{1}{2}[1 + erf(\frac{x-\mu}{\sqrt{2}\sigma})]$$

the cumulative distribution function for a gaussian with mean μ and standard deviation σ, the nth quantile is the probit function, inverse of ϕ. It can be

$< \rho >$ (MeV/cm^3)	Mean	Variance	Skewness	Excess Kurtosis	R 50	R 84	R 98
LHEP	28.1	189	2.33	7.87	0.87	0.89	1.27
QGSP	29.0	154	1.99	7.91	0.91	0.95	1.15
QGSP_BIC	27.8	152	1.76	5.20	0.90	0.95	1.18
QGSP_BERT	25.8	161	1.98	6.41	0.87	0.94	1.18
QGSP_BERT_HP	26.7	161	1.80	5.07	0.88	0.95	1.19
QGSC_BERT	27.4	135	1.66	5.24	0.91	0.96	1.14
FTF_BIC	27.6	191	1.63	3.70	0.87	0.96	1.20
FTFP_BERT	27.8	196	1.66	4.19	0.87	0.96	1.17
$< \rho^2 >$ (MeV^2/cm^6)	Mean ($\times 10^3$)	Variance ($\times 10^6$)	Skewness	Excess Kurtosis	R 50	R 84	R 98
LHEP	1.71	4.58	4.35	26.2	0.61	0.65	1.43
QGSP	1.72	3.39	5.37	53.3	0.70	0.74	1.25
QGSP_BIC	1.64	2.96	4.14	27.7	0.69	0.76	1.31
QGSP_BERT	1.51	3.14	4.37	29.3	0.65	0.72	1.32
QGSP_BERT_HP	1.55	3.00	3.98	25.1	0.65	0.75	1.37
QGSC_BERT	1.60	2.41	4.21	30.8	0.73	0.78	1.26
FTF_BIC	1.74	3.90	3.51	19.1	0.63	0.73	1.40
FTFP_BERT	1.78	4.11	3.72	22.8	0.62	0.76	1.34

Table 2: Statistics (see text) for the first and second moments on the energy density. Measurements obtained with 10000 events of π^+ with $E_{kin} = 20$ GeV.

expressed in terms of the error function:

$$\frac{x-\mu}{\sqrt{2}\sigma} = probit(p) = \sqrt{2}erf^{-1}(2p-1) \ , \ p = n/100$$

And thus:

$$G_n = \mu + \sigma \times \sqrt{2}probit(n/100) \tag{11}$$

For the energy density momenta, $R(50)$ and $R(84)$ are smaller then unity, while $R(98) > 1$, the distributions present a *core* that is more compact than the equivalent gaussian and have a very long (asymmetric) tail.

LHEP , QGSP and the FTF based models give higher values for the mean value of $< \rho >$ and $< \rho^2 >$.

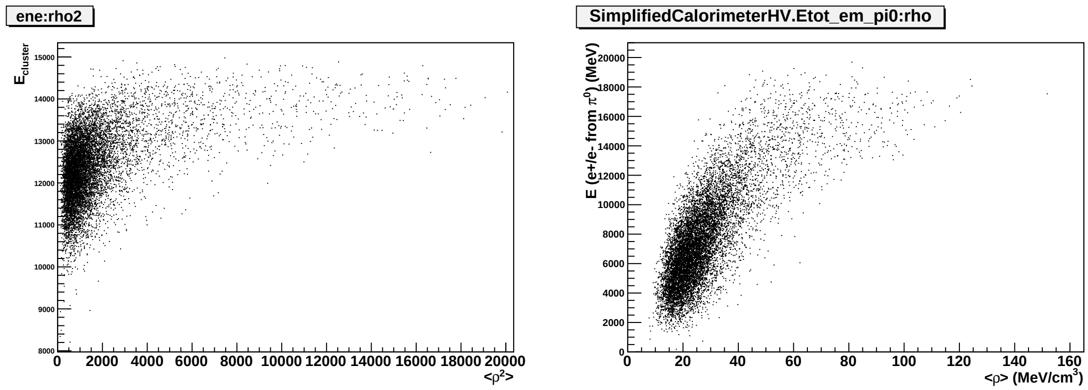

Figure 7: Left: correlation between the energy released in the calorimeter and the second moment in the energy density. Right: correlation between the energy released by the electromagnetic component of the shower and the first moment in the energy density. `LHEP` physics list.

For `LHEP` and the two Fritiof physics lists also the variance of the distribution is higher, indicating larger event-by-event fluctuations.

This is confirmed also analysing the tail of the distributions. The `LHEP` and `FTF_BIC` physics lists have a higher value of $R(98)$.

3.2 Moments related to the shower profile

The longitudinal shower profile is characterized by the *shower depth* and by the *length* of the shower: λ_{center} and the second moment in the longitudinal length, $< \lambda^2 >$.

Figure 8 shows the distributions of these moments for the different physics lists. As in the case of the energy density moments the distributions are characterized by a well defined *core* and a very long tail. The statistics (mean, variance, skewness, excess kurtosis and R ratios) are summarized in Table 3.

The shower center λ_{center} is found deeper inside the calorimeter for the Fritiof based model. `FTF_BIC` and `FTFP_BERT` show the highest value for this moment (respectively +6% and +7% with respect `QGSP`). The `LHEP` , `QGSP` and `QGSP_BIC` have, at the opposite, early starting showers. The Bertini code increases the shower depth and the `BERT` physics lists have mean value of

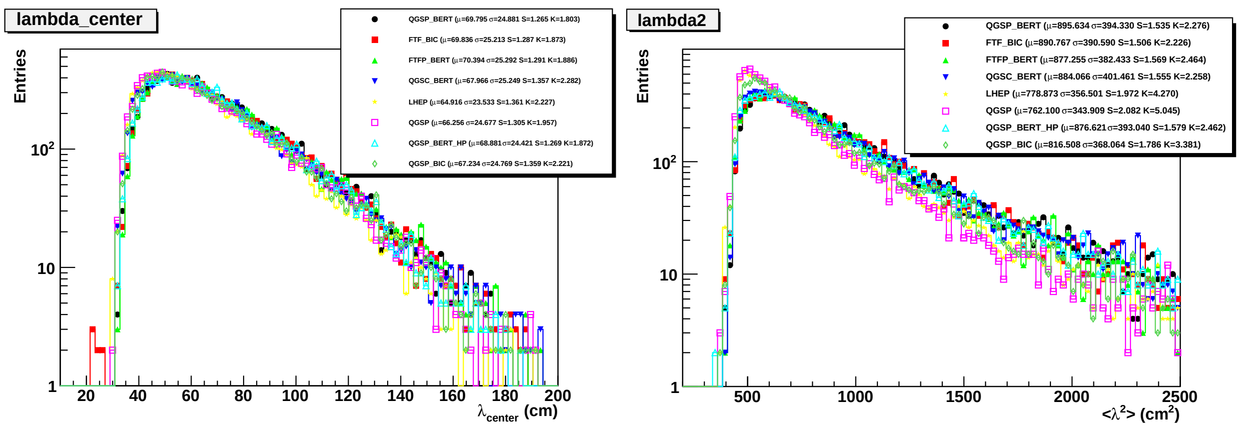

Figure 8: Shower center λ_{center} (left) and second moment on λ (right).

λ_{center} in the intermediate region. The variance of the distributions follows the same classification: `LHEP` , `QGSP` and `QGSP_BIC` shower depth fluctuates less with respect the other physics lists. From the analysis of the tail of the distributions (skewness, kurtosis and R ratios) we do not observe particular differences between physics lists, all values are quite similar to each other. The skewness and kurtosis are higher for the early showering models. This is due to a more compact *core* of the distribution (smaller variance) and to few events with higher values of λ_{center}. Kurtosis and skewness are indeed more sensitive to outliers in the distribution, with respect to the percentile ratios. For all physics lists the importance of the tail of the distribution is similar.

If λ_{center} is a measure of the shower depth, the second moment in the shower length $< \lambda^2 >$ is used to characterize the longitudinal dimension of the shower. From the right plot of Figure 8 it is possible to distinguish the different shape of the distribution of $< \lambda^2 >$ for the `QGSP` physics list. In this case the longitudinal profile is visibly more compact. Similarly to the case of shower depth the `LHEP` and `QGSP_BIC` physics lists have a smaller value for the mean of $< \lambda^2 >$: the showers are more compact in the longitudinal dimension. The other physics lists have higher mean values but, differently from what observed with λ_{center}, the Fritiof models do not present a particular enhancement of the longitudinal shower profile. Also in this case `LHEP` , `QGSP` and `QGSP_BIC` have smaller variance of the distribution of $< \lambda^2 >$ and the showers fluctuate less.

λ_{center} (cm)	Mean	Variance	Skewness	Excess Kurtosis	R 50	R 84	R 98
LHEP	65.8	591	1.39	2.44	0.91	0.97	1.17
QGSP	65.9	601	1.40	2.49	0.91	0.98	1.15
QGSP_BIC	67.4	619	1.35	2.11	0.91	0.98	1.15
QGSP_BERT	69.8	637	1.29	1.97	0.91	0.98	1.15
QGSP_BERT_HP	69.3	619	1.26	1.80	0.91	0.99	1.13
QGSC_BERT	68.6	663	1.32	2.04	0.91	0.98	1.16
FTF_BIC	69.9	633	1.29	1.92	0.91	0.98	1.15
FTFP_BERT	70.7	671	1.32	1.91	0.91	0.98	1.15
$< \lambda^2 >$ (cm^2)	Mean	Variance ($\times 10^3$)	Skewness	Excess Kurtosis	R 50	R 84	R 98
LHEP	826	246	3.51	18.5	0.80	0.83	1.30
QGSP	798	212	3.58	20.1	0.81	0.84	1.29
QGSP_BIC	853	239	3.15	14.7	0.81	0.86	1.28
QGSP_BERT	949	283	2.73	11.0	0.83	0.88	1.27
QGSP_BERT_HP	933	288	2.88	12.4	0.82	0.88	1.27
QGSC_BERT	942	293	2.75	10.7	0.82	0.88	1.29
FTF_BIC	942	276	2.82	11.8	0.83	0.88	1.27
FTFP_BERT	934	277	2.87	12.3	0.83	0.87	1.29

Table 3: Statistics (see text) for λ_{center} and the second λ moment. Measurements obtained with 10000 events of π^+ with $E_{kin} = 20$ GeV.

For what the longitudinal profile is concerned we can thus conclude that the use of Bertini or Fritiof models makes showers start later in the calorimeter (this is particularly true for the FTF physics lists) but also it makes them longer.

The lateral development of the showers is characterized by the first and second moment in the variable r (see equation 4). In this case there are clear differences between physics lists: Figure 9 shows the first (left) and second (right) moments on r. The distributions, characterized by a bell shape with a small tail towards higher values of the observable, have distinct mean values, summarized (together with variance, skewness and excess kurtosis) in Table 4.

We can observe that QGSP , LHEP and QGSP_BIC predict again the most compact showers . QGSC_BERT , QGSP_BERT_HP and FTF_BIC physics lists

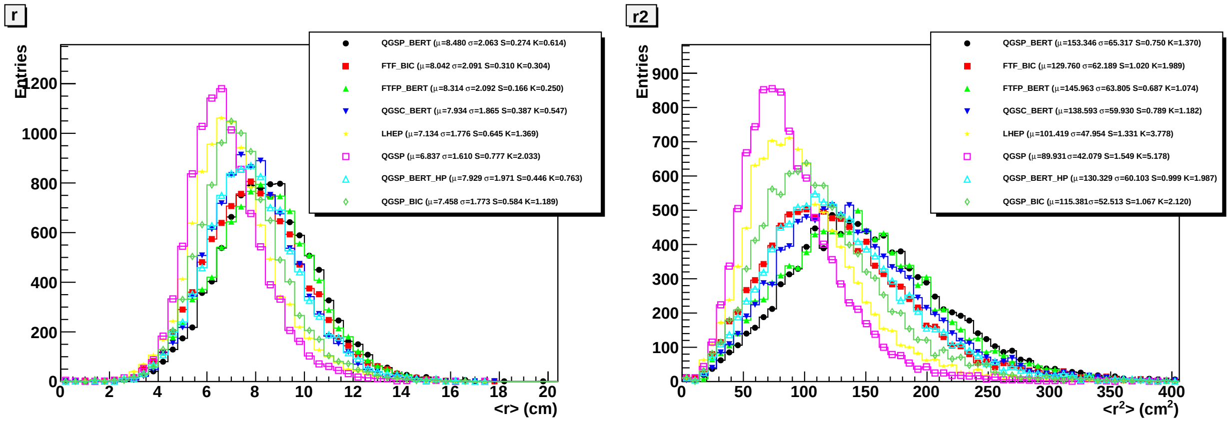

Figure 9: First (left) and second (right) moment on r.

have shower a bit wider in the radial dimension followed by FTFP_BERT and QGSP_BERT . The use of Bertini intra nuclear cascade code makes shower wider but, differently from the case of longitudinal profile, the FTF model does not play a particular role. This is expected since the Fritiof model is important to describe the forward-fast moving secondaries.

3.3 Moments related to the core and halo of the shower

The shower shape is mainly characterized by the moments in the longitudinal and lateral profile, however it is also useful to distinguish between the energy released in the *core* and in the *halo* of the shower. It is possible to group the cells in different ways to define those regions. For this study we decided to use the high granularity of the voxels and define two segmentation. A three dimensional one, f^{max} variables and a two dimensional segmentation (tower structure) f^{core} variables . Figure 10 shows the distributions for three f^{ax} moments (top) and the three f^{core} moments (bottom). Table 5 summarizes the mean value, variance, skewness and excess kurtosis for the different physics lists.

The distributions are all very similar, only the LHEP , QGSP and QGSP_BIC physics lists present distributions with higher mean value and lower variance. This is again a symptom of more compact shower shapes. A higher fraction of the shower energies indeed is released in a relatively smaller number of

$< r >$ (cm)	Mean	Variance	Skewness	Excess Kurtosis
LHEP	7.15	3.21	0.68	1.47
QGSP	6.86	2.66	0.76	1.93
QGSP_BIC	7.46	3.29	0.65	1.36
QGSP_BERT	8.52	4.25	0.26	0.50
QGSP_BERT_HP	7.91	3.93	0.42	0.85
QGSC_BERT	7.90	3.61	0.32	0.47
FTF_BIC	8.04	4.42	0.32	0.44
FTFP_BERT	8.31	4.45	0.18	0.19
$< r^2 >$ (cm^2)	Mean	Variance ($\times 10^3$)	Skewness	Excess Kurtosis
LHEP	102	2.40	1.40	4.05
QGSP	91	1.82	1.67	9.27
QGSP_BIC	115	2.91	1.24	3.09
QGSP_BERT	154	4.24	0.67	1.02
QGSP_BERT_HP	130	3.61	1.04	2.36
QGSC_BERT	137	3.69	0.82	1.69
FTF_BIC	130	3.92	1.01	1.94
FTFP_BERT	146	4.13	0.65	0.79

Table 4: Statistics (see text) for the first and the second moment on the r. Measurements obtained with 10000 events of π^+ with $E_{kin} = 20$ GeV.

voxels. This result is in agreement with the conclusions we obtained from the analysis of the longitudinal and lateral profile moments.

Finally we can consider the increase of the fraction of energy collected in larger and larger volumes, i.e. the increase in f^{max} (f^{core}) moving from a $2 \times 2 \times 2$ (2×2) configuration to a $5 \times 5 \times 5$ (5×5). The results are shown in Figure 11. From left plot we can see that a relatively large fraction of the shower energy (between 60% and 70%) is already contained in a 2×2 towers, extending the tower to 3×3 collects about three quarter of the shower energy and the larger towers (5×5) allows us to increase the collected energy of only an additional 10%. With f^{core} we are integrating the shower profile along the longitudinal direction: we can see that the shower is composed of a compact *core* where the majority of the energy released and a *halo* with small importance: far away from the shower center a small amount of

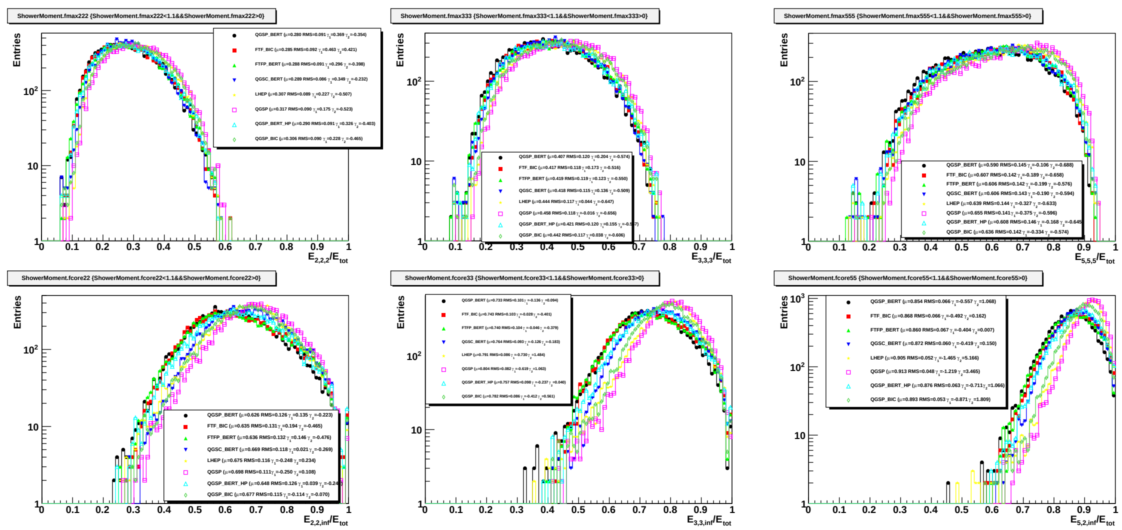

Figure 10: Energy fractions moments calculated with sliding window: $f^{max}_{2,2,2}$, $f^{max}_{3,3,3}$, $f^{max}_{5,5,5}$ (top row) and $f^{core}_{2,2}$, $f^{core}_{3,3}$, $f^{core}_{5,5}$ (bottom row).

energy is released on a large volume. We can give the same conclusions if we consider the three dimensional variable f^{max}: more than a quarter of the shower energy is released in a small volume (in our case $f^{max}_{2,2,2}$ corresponds to a cube of volume 10^3 cm^3).

From Table 5 and Figures 10 and 11 we can observe that, with the exclusion of `LHEP` , `QGSP` and `QGSP_BIC` all physics lists are quite similar.

3.4 Behavior of Moments

The characterization of showers via moments is only weakly dependent on the voxel dimensions. In addition the moments show a *smooth* behavior as a function of the primary energy.

Figure 12 shows the dependence of the lateral and longitudinal moments r, r^2, λ^2, λ_{center} as a function of the voxel dimension. For the same simulations the shower dimension moments are calculated for different voxel sizes. The ratio of the calculated moments with respect to a reference mesh size (with cubic voxels of 5 cm linear dimension) are shown. Left plot shows the longitudinal moments (λ_{center} in blue and $< \lambda^2 >$ in red). In both cases there is a very weak dependence on the voxel dimension. The plots on the

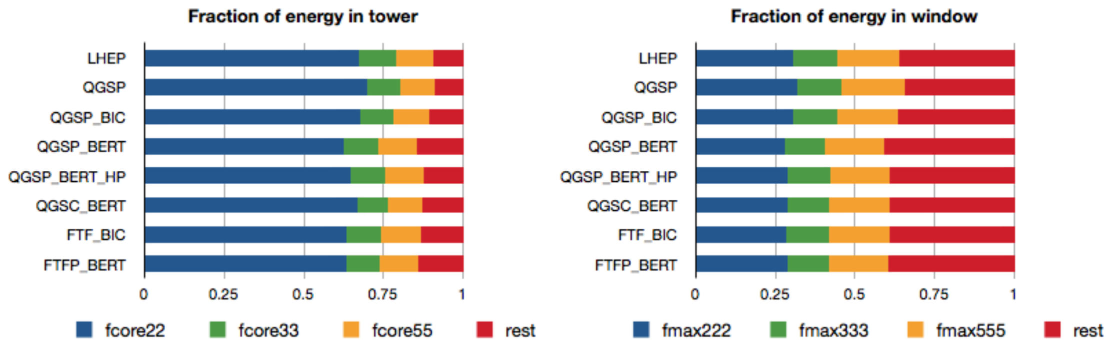

Figure 11: Division of the shower energy in subsequently bigger towers (left) and in three dimensional windows (right).

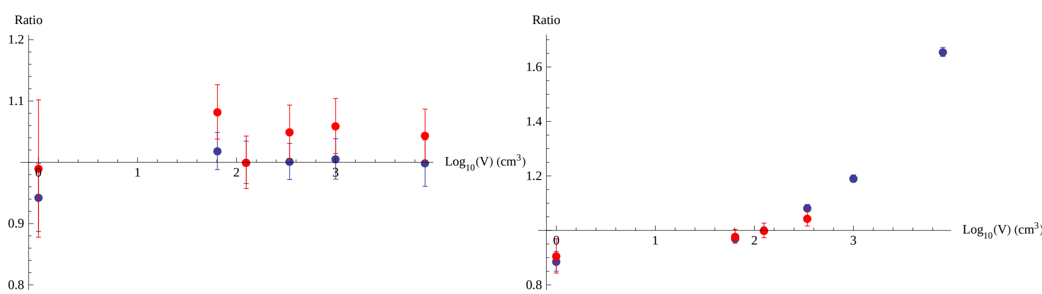

Figure 12: Relative variations of shower moments as a function of voxel dimension with respect the reference voxel size ($5 \times 5 \times 5$ cm^3). Left: λ_{center} (blue) and $< \lambda^2 >$ (red). Right: $< r >$ (blue) and $< r^2 >$ (red).

$f^{max}_{3,3,3}$	Mean	Variance ($\times 10^{-2}$)	Skewness	Excess Kurtosis
LHEP	0.444	1.37	0.04	-0.65
QGSP	0.458	1.39	-0.01	-0.66
QGSP_BIC	0.442	1.17	0.04	-0.61
QGSP_BERT	0.407	1.43	0.20	-0.57
QGSP_BERT_HP	0.421	1.44	0.15	-0.57
QGSC_BERT	0.418	1.31	0.13	-0.51
FTF_BIC	0.417	1.40	0.20	-0.37
FTFP_BERT	0.419	1.41	0.12	-0.55
$f^{core}_{3,3}$	Mean	Variance ($\times 10^{-2}$)	Skewness	Excess Kurtosis
LHEP	0.791	0.74	-0.73	1.47
QGSP	0.804	0.66	-0.62	1.05
QGSP_BIC	0.782	0.75	-0.41	0.56
QGSP_BERT	0.733	1.01	-0.13	0.10
QGSP_BERT_HP	0.757	0.97	-0.24	0.04
QGSC_BERT	0.764	0.86	-0.12	-0.18
FTF_BIC	0.743	1.07	-0.02	-0.39
FTFP_BERT	0.740	1.09	-0.04	-0.38

Table 5: Statistics (see text) for the $f^{max}_{3,3,3}$ and $f^{core}_{3,3}$ moments. Measurements obtained with 10000 events of π^+ with $E_{kin} = 20$ GeV.

right show the dependence for the lateral moments. In this case a stronger dependence is visible at large voxel volumes. Between $< r >$ and $< r^2 >$ the latter has a smaller dependence at small and moderate voxel sizes. This is an important result: with voxels of moderate dimensions, the characteristics of the shower do not depend on the read-out geometry used to calculate the moments. They are sensitive to the physics of the shower and not to the detector segmentation.

The distributions of the moments are characterized by long tails (see, for example, Figure 8). Even if the distributions cannot be described by a simple analytical form, they are regular as a function of the primary energy as shown in Figure 13. The figure shows a simplified Whisker plot for one particular moment (λ_{center}) for different primary beam energies. The star is the position of median of the distribution, while the full dot represents the position of the mean of the distribution. The error bars are the first and third quartile distribution. The distribution shapes are well behaved as a function of the beam energy and statistical error on the sample mean are small enough with 5000 events.

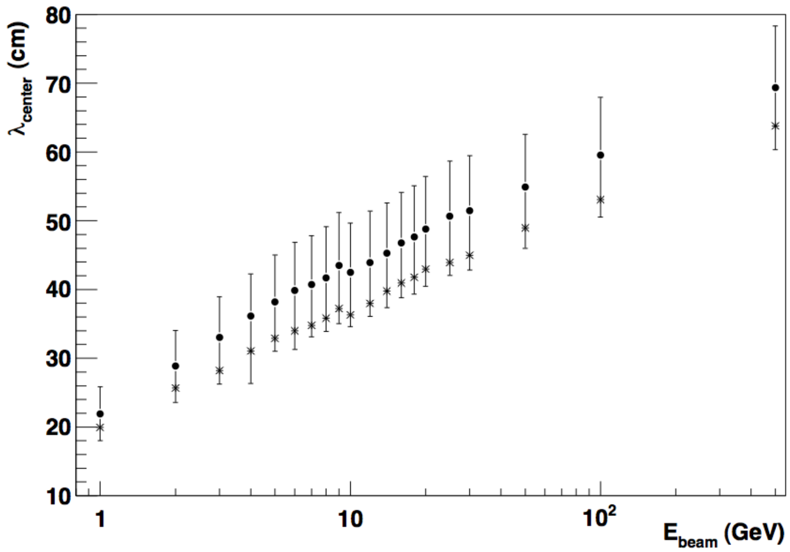

Figure 13: Whisker plots for λ_{center} distributions as a function of beam energy. See text for details.

4 Conclusions

We have presented a method to characterize the hadronic showers. Relying on a highly segmented calorimeter we have constructed some observables that characterize the shower shape and its composition. From the analysis of ρ, f^{core} and f^{max} we have shown that the hadronic showers are characterized by a relatively compact *core* with high energy density and a low energy density *halo*.

We have introduced the variables λ_{center}, $< \lambda^2 >$, $< r >$ and $< r^2 >$ that can summarize the longitudinal and lateral profile of the showers.

Our method gives the same conclusions as discussed in [1] [2] and is thus equivalent with the results obtained in the past. However the use of shower moments allows for a more detailed and quantitative description of the shower shapes.

References

[1] A. Ribon et al.; Hadronic shower shapes studies in Geant4: Update; 2008 (CERN); CERN-LCGAPP-2008-01

[2] A. Ribon et al.; Hadronic Shower Shape Studies in Geant4; 2007 (CERN); CERN-LCGAPP-2007-02

[3] T. Barillari et al.; Local Hadron Calibration; 2008 (CERN); ATL-LARG-PUB-2009-001

A Appendix: Technical implementation

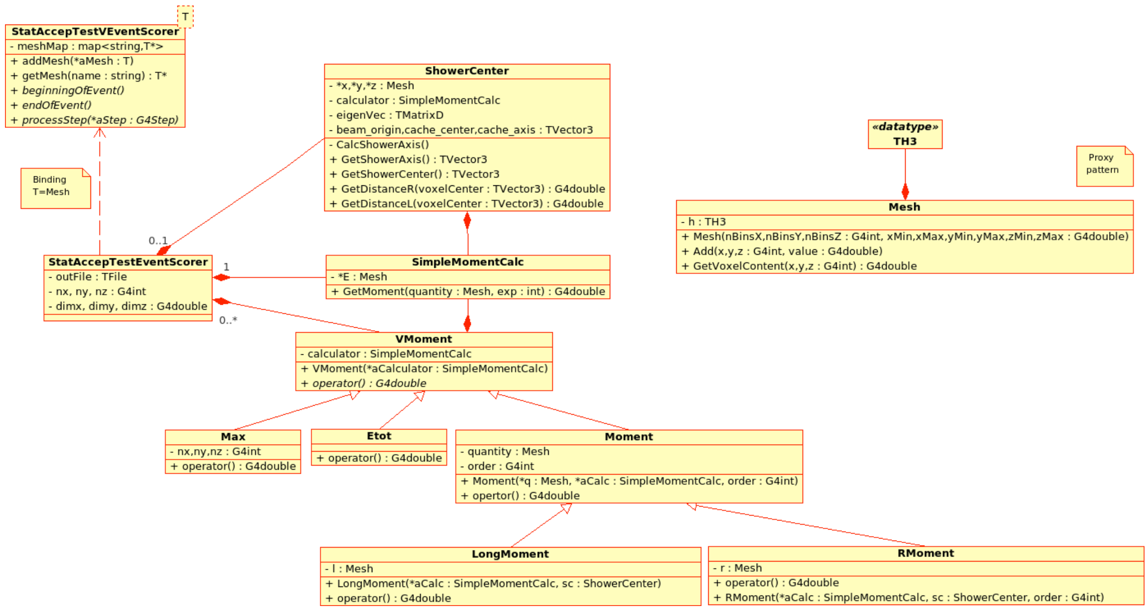

Figure 14: Class diagram for the shower moment calculations.

One of the main components to calculate the shower moments is the ability to accumulate, in a three-dimensional structure of *voxels*, the energy deposits. This is implemented through a 3D histogram. The class *Mesh* implements a proxy pattern to the underlying structure implementing the accumulation. In this case a 3D ROOT histogram. The use of the proxy pattern allows for a possible replacement of the TH3 object with a user-defined histogramming object.

The class *SimpleMomentCalc* implements the main logic of the calculation of shower moments, via the call to the *GetMoment* function:

```
G4double SimpleMomentCalc::GetMoment( Mesh& quantity, G4int exp ) {
// implements the calculation
//<quantity^exp> = Sum_i E_i*q_i^exp / Sum_i E_i
}
```

This class holds the mesh of the energy deposits for each voxel, it thus allows to calculate the totally energy of the cluster.

The *VMoment* class implements the interface for a generic moment, implementing a functor pattern. It holds a reference to the *SimpleMomentCal* instance associated to the current cluster. The class *Moment* implements the generic moment calculation implementing the function:

```
G4double operator()() {
return calculator->GetMomet( *quantity , order );
}
```

The *quantity* parameter of type Mesh and the *order* (of type integer) are moment specific. For example the *LongMoment* and *RMoment* classes implement the longitudinal and lateral shower moments.

The class *ShowerCenter* implements the principal component analysis on the mesh of the energy deposits for each voxel. It uses ROOT classes and holds a *TVector3* representing the shower center and one *TVector3* representing the shower axis. The class also implements the calculation of the R and λ for a given point in space with respect shower center and shower moment. The class uses an object of type *SimpleMomentCalc* to access the energy of the cluster.

A typical example of the use of shower moments is shown in the following pseudo-code example. If a given observable o can be defined for each voxel it is enough to implement a class, inheriting from *Moment* that creates a *Mesh* object containing the observable o. The code of *RMoment* is a good and complete example. The analysis is performed in this way:

```
beginOfEvent() {
// Create an empty Mesh with the desired granularity
Energy = new Mesh( divisions );
aQuantity = new Mesh( divisions );
}

processStep( G4Step* aStep) {
//for each step accumulate the energy :
Energy->Add( x, y, x, aStep->GetEnergyDeposit() );
aQuantity->Add( x, y, x, somederivedquantity );
}

endOfEvent() {
SimpleMomentCalc smc( Energy );
```

```
//If shower center and axis are needed:
ShowerCenter sc( smc , BeamOrigin );
sc.CalcShowerAxis();

MyMoment mom( aQuantity , &smc, 1);
MyMoment mom2(aQuantity, &smc , 2);

G4double firstOrderMomentOfMom = mom();
G4double secondOrderMomentOfMom = mom2();
 }
```

The use of the moments is general enough to allow for calculating several quantities even if these do not follow strictly the definition of moment. For example the class *RBinEsum* calculates the energy in all voxels with $r_{min} < r < r_{max}$. The calculation uses *EConditionalSum* that implements the sum of the energies in a given set of voxels. Using *RBinEsum* as an example it is possible to define the summation of energies for any pattern of voxels. Another example of the flexibility of the use of moments is shown by *Max* class: it searches for the set of $n_x \times n_y \times n_z$ adjacent voxels that contain the maximum energy.

Class Name	Parameters	Function
Etot		Calculates total energy of the shower
EConditionalSum	Mesh of 0 or 1	Calculates the sum of energies in a set of voxels
LongMoment	ShowerCenter vector	Calculates $< \lambda^2 >$
Max	n_x, n_y, n_z	Searches the set of $n_x \times n_y \times n_z$ adjacent voxels containing the maximum energy
RBinEsum	ShowerCanter vector, r_{min}, r_{max}	Calculates the energy in voxels with $r_{min} < r < r_{max}$
Moment	a Mesh, an order	Calculates the general moment $< m^o >$
RMoment	ShowerCenter vector, an order	Calculates $< r^o >$

Table 6: List of moments classes used by default in the application. These can be used as an example to extend the application with new moments.